Structure of trichodiene synthase from *Fusarium sporotrichioides* provides mechanistic inferences on the terpene cyclization cascade

Michael J. Rynkiewicz*, David E. Cane†, and David W. Christianson*‡

*Department of Chemistry, University of Pennsylvania, Philadelphia, PA 19104-6323; and †Department of Chemistry, Brown University, Providence, RI 02912

Edited by Douglas C. Rees, California Institute of Technology, Pasadena, CA, and approved September 25, 2001 (received for review June 19, 2001)

The x-ray crystal structure of recombinant trichodiene synthase from *Fusarium sporotrichioides* has been determined to 2.5-Å resolution, both unliganded and complexed with inorganic pyrophosphate. This reaction product coordinates to three Mg^{2+} ions near the mouth of the active site cleft. A comparison of the liganded and unliganded structures reveals a ligand-induced conformational change that closes the mouth of the active site cleft. Binding of the substrate farnesyl diphosphate similarly may trigger this conformational change, which would facilitate catalysis by protecting reactive carbocationic intermediates in the cyclization cascade. Trichodiene synthase also shares significant structural similarity with other sesquiterpene synthases despite a lack of significant sequence identity. This similarity indicates divergence from a common ancestor early in the evolution of terpene biosynthesis.

Sesquiterpene synthases (also known as terpenoid cyclases) catalyze the conversion of a universal substrate, farnesyl diphosphate, into more than 300 known terpene cyclization products with different structures and stereochemistries (1–5). It is striking that such broad product diversity is achieved by a structurally homologous group of enzymes, each of which typically has evolved to catalyze a single cyclization reaction with exquisite structural and stereochemical precision. Some cyclases, however, exhibit more relaxed precision (6–10). Facile mutation and evolution of terpenoid cyclases represents an effective strategy to maximize product diversity in terpenoid biosynthesis.

All sesquiterpene synthases characterized to date are soluble proteins with monomer M_r = 40–60 kDa and require divalent metal cations, usually Mg^{2+} and sometimes Mn^{2+}, as cofactors for catalysis. Most but not all sesquiterpene synthases are active as monomers. Metal ion(s) bind to the so-called aspartate-rich motif DDXX(D,E), that is found in all known terpene cyclase amino acid sequences (4, 5, 11). The x-ray crystal structures of three cyclases have been solved to date: pentalenene synthase from *Streptomyces* UC5319 (12), 5-*epi*-aristolochene synthase from *Nicotiana tabacum* (13), and aristolochene synthase from *Penicillium roqueforti* (14). Despite a lack of significant overall sequence identity, these enzymes all share the "terpenoid synthase fold" (12), which is also shared by avian farnesyl diphosphate synthase (15) and human squalene synthase (16). Structural similarity maintained in the face of broad synthetic diversity indicates divergence from a common ancestor early in the evolution of terpene biosynthesis. Interestingly, two evolutionarily distinct folds are observed in other terpene biosynthetic enzymes: an unrelated α-helical fold exhibited by squalene-hopene cyclase (4) and an α/β fold exhibited by undecaprenyl diphosphate synthase (17).

Trichodiene synthase is a sesquiterpene cyclase that catalyzes the formation of trichodiene in the biosynthesis of antibiotics and mycotoxins (refs. 3 and 18; Fig. 1). We now report x-ray crystal structures of recombinant trichodiene synthase from *Fusarium sporotrichioides* (19) and its complex with pyrophosphate. These structures reveal an unusual dimeric terpenoid cyclase that undergoes a substrate-induced conformational change to trigger the cyclization cascade. Additionally, these structures provide a foundation for understanding the results of numerous enzyme mechanistic and site-directed mutagenesis experiments (20–24).

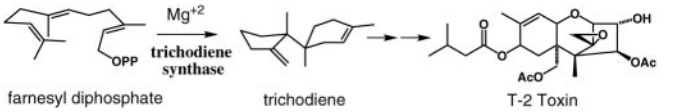

Fig. 1. Cyclization of farnesyl diphosphate to trichodiene is the first committed step in the biosynthesis of nearly 100 different trichothecene toxins and antibiotics produced by as many as 10 genera of fungi, of which T-2 toxin in *F. sporotrichioides* is an example. OPP, diphosphate.

Materials and Methods

Crystal Structure Determination. Trichodiene synthase was purified as described (20), omitting the initial ammonium sulfate precipitation step. Additionally, after anion exchange chromatography, the enzyme was loaded onto a methyl-HIC column (Bio-Rad) equilibrated with 10 mM Tris, pH 7.8, 5 mM $MgCl_2$, 5 mM β-mercaptoethanol, 15% glycerol, and 1.5 M ammonium sulfate. The enzyme was eluted with a step gradient of 1 M ammonium sulfate for 2 column volumes and applied to a Superdex 200 column (Amersham Pharmacia Biotech) equilibrated with 10 mM Tris, pH 7.8, 5 mM $MgCl_2$, and 5 mM β-mercaptoethanol. Crystals were grown from hanging drops of 4 μl of enzyme (20 mg/ml) and 2 μl of precipitant buffer (0.1 M Hepes, pH 6.9, 50 mM $CaCl_2$, and 6–10% (wt/vol) polyethylene glycol 8,000) equilibrated over a reservoir of 0.5 ml of precipitant buffer. Crystals appeared within a week, grew to 0.5 × 0.5 × 0.3 mm, and belonged to space group $P3_121$ (a = b = 122.2 Å, c = 151.2 Å; two molecules in the asymmetric unit, solvent content = 66%).

For derivatization, crystals were transferred to a solution of 0.1 M Hepes, pH 6.9, 10% polyethylene glycol 8,000, and 0.2 mM lead acetate for 2 h. For cryoprotection, the crystals were transferred gradually to a buffer containing 0.1 M Hepes, pH 6.9, 10% polyethylene glycol 8,000, and 25% glycerol or ethylene glycol. Initial x-ray diffraction data sets used to generate initial electron density maps (native-1 and lead acetate) were collected at the Stanford Linear Accelerator Center (beamline 7-1). A 2.5-Å resolution data set (native-2) was collected at the Advanced Photon Source (Structural Biology Center-Collaborative Access Team). Crystals of the trichodiene synthase-pyrophos-

This paper was submitted directly (Track II) to the PNAS office.

Data deposition: The atomic coordinates and structure factors for native trichodiene synthase and the trichodiene synthase-pyrophosphate complex have been deposited in the Protein Data Bank, www.rcsb.org (PDB ID codes 1JFA and 1JFG, respectively).

See commentary on page 13479.

‡To whom reprint requests should be addressed. E-mail: chris@rock.chem.upenn.edu.

The publication costs of this article were defrayed in part by page charge payment. This article must therefore be hereby marked "*advertisement*" in accordance with 18 U.S.C. §1734 solely to indicate this fact.

Table 1. Data collection statistics

Data set	Resolution, Å	Reflections, measured/unique	Completeness %, overall/outer shell	R_{merge},* overall/outer shell	R_{iso}†	Number of sites	Phasing power‡	Figure of merit,§ 2.8 Å, before/after density modification
Native-1	2.7	266462/36943	99.5 (99.7)	0.047 (0.335)				
Native-2	2.5	386732/45629	99.1 (94.5)	0.069 (0.310)				
Lead acetate	2.7	237535/36235	99.6 (100.0)	0.061 (0.305)	0.217	4	1.11	0.33/0.74
Diphosphate	2.5	193928/46785	98.1 (99.6)	0.069 (0.306)				

*$R_{merge} = \Sigma|I - \langle I\rangle|/\Sigma I$, where I is the observed intensity and $\langle I\rangle$ is the average intensity for replicate data.
†$R_{iso} = \Sigma(|F_{PH}| - |F_P|)/\Sigma |F_P|$, where $|F_{PH}|$ and $|F_P|$ are the structure factor amplitudes of the derivative and native data sets, respectively.
‡Phasing power $= \langle F_H\rangle/E$, where $\langle F_H\rangle$ is the root mean square heavy atom structure factor, and E is the residual lack of closure.
§Figure of merit $= \Sigma\langle\cos \Delta\alpha_j\rangle/n$, where $\Delta\alpha_j$ is the error in the phase angle for reflection j, and n is the number of reflections.

phate complex were prepared by soaking in a solution of 0.1 M Hepes, pH 6.9, 10% polyethylene glycol 8,000, 1 mM $MgCl_2$, and 2 mM sodium pyrophosphate for 2 h. Crystals were isomorphous with those of the native enzyme, and data were collected at the National Synchrotron Light Source (beamline X12C). All data were scaled and integrated by using the programs DENZO and SCALEPACK (25). Data collection statistics are reported in Table 1.

Initial phases were calculated by single isomorphous replacement with anomalous scattering using two lead sites per monomer. Heavy atom positions were refined with MLPHARE (26), and density modification was performed with DM (26, 27). Each polypeptide chain and ordered solvent molecules were fit into the resulting electron density maps with O (28) and then refined against all data with CNS (29). The C termini (R355-E374) are disordered in both monomers, and the N terminus (M1–F4) of monomer B is disordered, thus these residues are excluded from the final model. Strict noncrystallographic symmetry constraints were used initially and relaxed into appropriately weighted restraints as guided by R_{free}. The noncrystallographic symmetry axis is the dyad axis of the dimer. The final model has excellent geometry with 92 and 8% of residues adopting most favored and additionally allowed conformations, respectively.

The structure of the trichodiene synthase-pyrophosphate complex was solved by difference Fourier methods using the unliganded structure as a starting point. Monomer B exhibited clear electron density for three Mg^{2+} ions and one pyrophosphate molecule; monomer A did not, possibly because of an active site partially blocked by crystal lattice interactions. In refinement, noncrystallographic symmetry restraints were not applied to polypeptide segments exhibiting pyrophosphate-induced conformational changes (residues 1–29, 99–105, 229–242, and 300–335). Final refinement statistics are recorded in Table 2.

Modeling. Farnesyl diphosphate, intermediate carbocation, and trichodiene structures were generated with MACROMODEL (30), and a Monte Carlo conformational search yielded minimum energy conformations for each. The search was constrained to conformations that would support the reaction coordinates of C–C bond formation previously determined for trichodiene biosynthesis. For example, the C1 and C6 atoms of farnesyl diphosphate, which form a six-membered ring in the first electrophilic cyclization, were constrained to a separation of 3.5 Å. The resulting structures were docked manually into the active site by using O. Finally, 30 cycles of rigid body and 200 cycles of conjugate gradient energy minimization with CNS optimized the structure of each enzyme-ligand model. In energy minimizations, pyrophosphate, Mg^{2+} ions, and associated water molecules were fixed, and a harmonic restraint of 10 kcal·mol^{-1}·Å^{-2} was applied to the carbon portions of the substrate or intermediate. Nonbonded interactions in the crystal lattice were included in the minimization, but no other constraints were applied to the protein atoms. Changes of as much as 0.5 Å were noted in the side chain positions of D100, D101, K232, D236, Y295, and Y305 after energy minimizations, but no changes in backbone positions were observed.

Results and Discussion

Structure of Native Trichodiene Synthase. The trichodiene synthase structure is formed by 17 α-helices (Fig. 2*A*), six of which (C, D, G, H, I, and J) define a conical and hydrophobic active site cleft. The aspartate-rich motif starting at residue 100, DDSKD, is located at the C-terminal end of helix D (Fig. 2*A*). Mutagenesis studies demonstrate that D100 and D101 are important for catalytic activity (21). On the opposite wall of the active site cavity, at the C-terminal end of helix J, is the "basic motif" starting at residue 302, DRRYR (Fig. 2*A*). Mutagenesis studies of R304, Y305, and R306 in this motif similarly indicate importance for catalysis (20).

Native and recombinant trichodiene synthases are homodimers (19), and the dimeric quaternary structure shown in Fig. 2*B* is the first observed for a terpenoid cyclase. Farnesyl diphosphate synthase is also a homodimer (15), but the dimer interface differs substantially from that observed in trichodiene synthase. Moreover, active sites are oriented in a parallel fashion in the farnesyl diphosphate synthase dimer and in an antiparallel fashion in the trichodiene synthase dimer. Additionally, the dimer interface in trichodiene synthase does not overlap with the domain-domain interface between the N-terminal domain and

Table 2. Refinement statistics

Structure	Native	Diphosphate
Protein atoms	5,846	5,882
Solvent atoms	283	310
Ligand atoms	0	12
Resolution range, Å	30–2.5	25–2.5
Data cutoff, σ	0	0
No. of reflections, work/free	37,480/3,196	38,849/3,333
R/R_{free}	0.218/0.250	0.220/0.257
Rms deviations		
Bonds, Å	0.007	0.012
Angles, °	1.2	1.4
Dihedrals, °	18.6	19.5
Impropers, °	0.7	0.9
Average B factors, Å^2 (rms deviation)		
Main chain	43.9 (1.2)	34.2 (1.0)
Side chain	45.5 (1.7)	35.6 (1.7)
Ligand	—	50.4

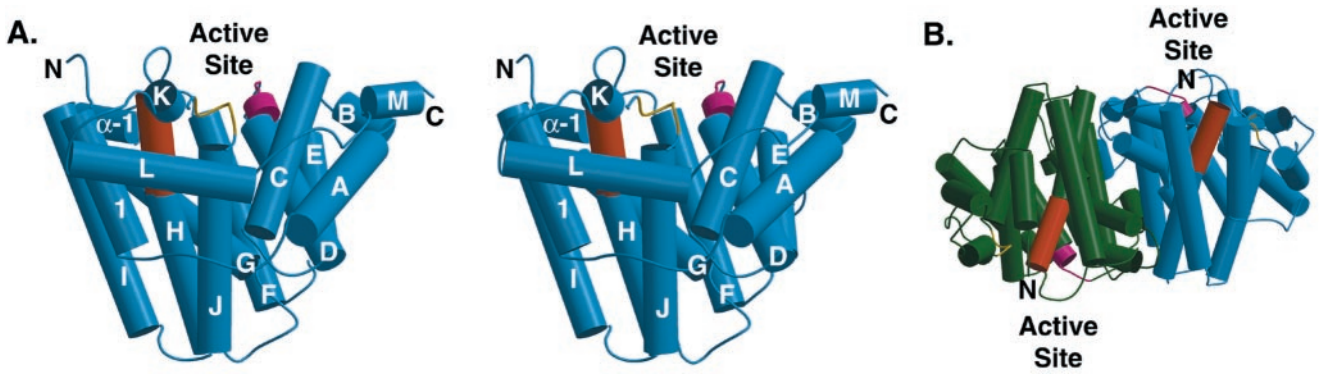

Fig. 2. (*A*) Stereoplot of the trichodiene synthase monomer. The aspartate-rich motif beginning at residue 100 (DDSKD) on the upper wall of the active site is magenta, and the second metal-binding motif starting at residue 223 (WVNDLMSFYKE) is orange. The basic motif beginning at residue 302 (DRRYR) is yellow. Helical segments are designated by the convention used for farnesyl diphosphate synthase (15) and contain the following residues: 1, 6–19; A, 29–48; B, 50–55; C, 60–77; D, 83–102; D1, 107–110; D2, 113–119; E, 126–139; F, 144–164; G, 177–194; H, 207–233; α-1, 243–251; I, 255–277; J, 282–301; K, 307–311; L, 320–336; M, 348–353. (*B*) Structure of the trichodiene synthase dimer. Important motifs are colored as in *A*. The figure was generated with MOLSCRIPT (37) and RASTER 3D (38, 39).

the cyclase domain in 5-*epi*-aristolochene synthase (13). The dimer interface of trichodiene synthase buries a total of 5,300 Å^2 solvent-exposed surface area (≈50% is hydrophobic).

A search using the combinatorial extension protocol (31) reveals significant structural similarity among the terpenoid synthases despite only 6–15% sequence identity (Fig. 3). Notably, all these enzymes use farnesyl diphosphate as either substrate or product, and all these enzymes catalyze chemical reactions with highly reactive carbocations. Therefore, in divergent evolution from a common ancestor, this α-fold evolved to accommodate different reactions by mutation of the active site contour, i.e., the template for farnesyl diphosphate binding.

Trichodiene Synthase-Diphosphate Complex. The electron density map of the trichodiene synthase-pyrophosphate complex reveals three bound Mg^{2+} ions and one molecule of inorganic pyrophosphate in monomer B (Fig. 4). Two metal-binding regions are evident in the active site. First, the carboxylate of D100 (the first residue of the aspartate-rich motif on helix D) coordinates to $Mg^{2+}{}_A$ and $Mg^{2+}{}_C$ with *syn*,*syn*-bidentate geometry. The corresponding aspartate also coordinates to $Mg^{2+}{}_A$ and $Mg^{2+}{}_C$ in 5-*epi*-aristolochene synthase (13) and farnesyl diphosphate synthase (32) and Sm^{+3} in aristolochene synthase (14). No other residues in the aspartate-rich motif of trichodiene synthase participate directly in metal binding.

The second metal-binding region of trichodiene synthase is comprised of N225, S229, and E233 on helix H, which coordinate to $Mg^{2+}{}_B$. The corresponding region is also found in 5-*epi*-aristolochene synthase, where D444, T448, and E452 coordinate to $Mg^{2+}{}_B$ (13). These residues are part of a consensus sequence, V(V,I)(N,D)D(L,I,V)Y(S,T), identified in all known monoterpene, sesquiterpene, and diterpene synthase sequences (33). Additionally, crystal structures show that a nearby, highly conserved glutamate completes the $Mg^{2+}{}_B$ binding site (E233 in trichodiene synthase and E452 in 5-*epi*-aristolochene synthase). PILEUP analysis of a group of 32 monoterpene, sesquiterpene, and diterpene synthases reveals that this glutamate is part of a highly conserved, 11-amino acid consensus sequence, (L,V)(V, L,A)(**N**,**D**)D(L,I,V)X(**S**,**T**)XXX**E**; residues in bold define a complete $Mg^{2+}{}_B$ binding site. The Mg^{2+} ions mediate a complex network of enzyme-pyrophosphate interactions (Fig. 4*B*). However, a diphosphate moiety seems to be required for high affinity metal binding, because metal binding is not observed in the empty active site of monomer A or in monomers A and B of the unliganded enzyme.

In addition to multiple metal coordination interactions, py-

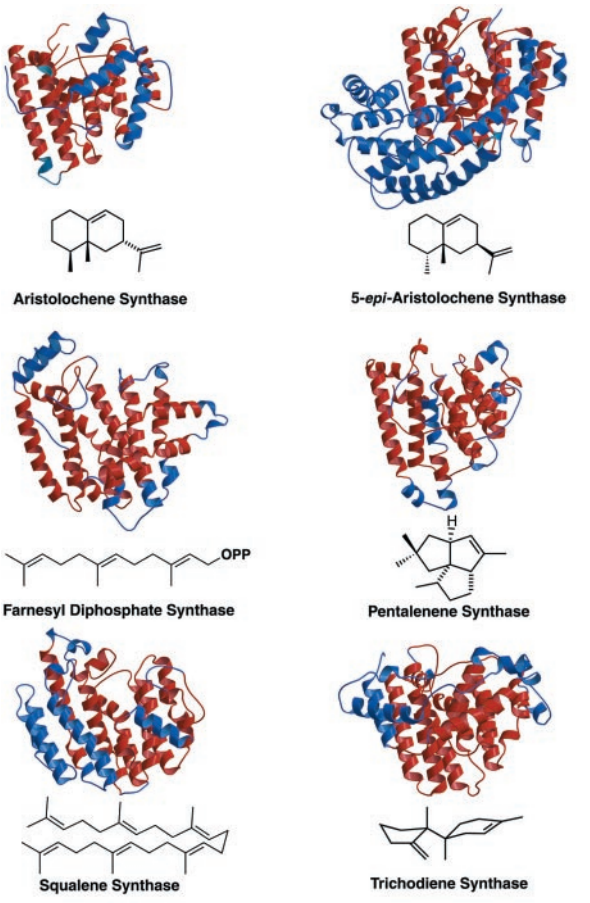

	FDPS	AS	EAS	PS	SQS
TS	3.9 Å (238)	4.0 Å (205)	3.2 Å (212)	3.3 Å (251)	3.6 Å (192)
FDPS	-	3.7 Å (193)	3.4 Å (244)	2.9 Å (159)	3.5 Å (215)
AS	-	-	3.1 Å (222)	3.0 Å (291)	3.6 Å (191)
EAS	-	-	-	3.2 Å (238)	3.6 Å (227)
PS	-	-	-	-	3.4 Å (191)

Fig. 3. Structural similarity of terpene synthases. Regions of structural similarity (red) comprise the core terpenoid synthase fold. At the bottom are the rms deviation of C^α atoms and the number of structurally similar residues (in parentheses). The enzymes are trichodiene synthase (TS), farnesyl diphosphate synthase (FDPS, PDB code 1UBW), aristolochene synthase (AS, PDB code 1DI1), 5-*epi*-aristolochene synthase (EAS, PDB code 5EAT), pentalenene synthase (PS, PDB code 1PS1), and squalene synthase (SQS, PDB code 1EZF). OPP, diphosphate.

BIOCHEMISTRY

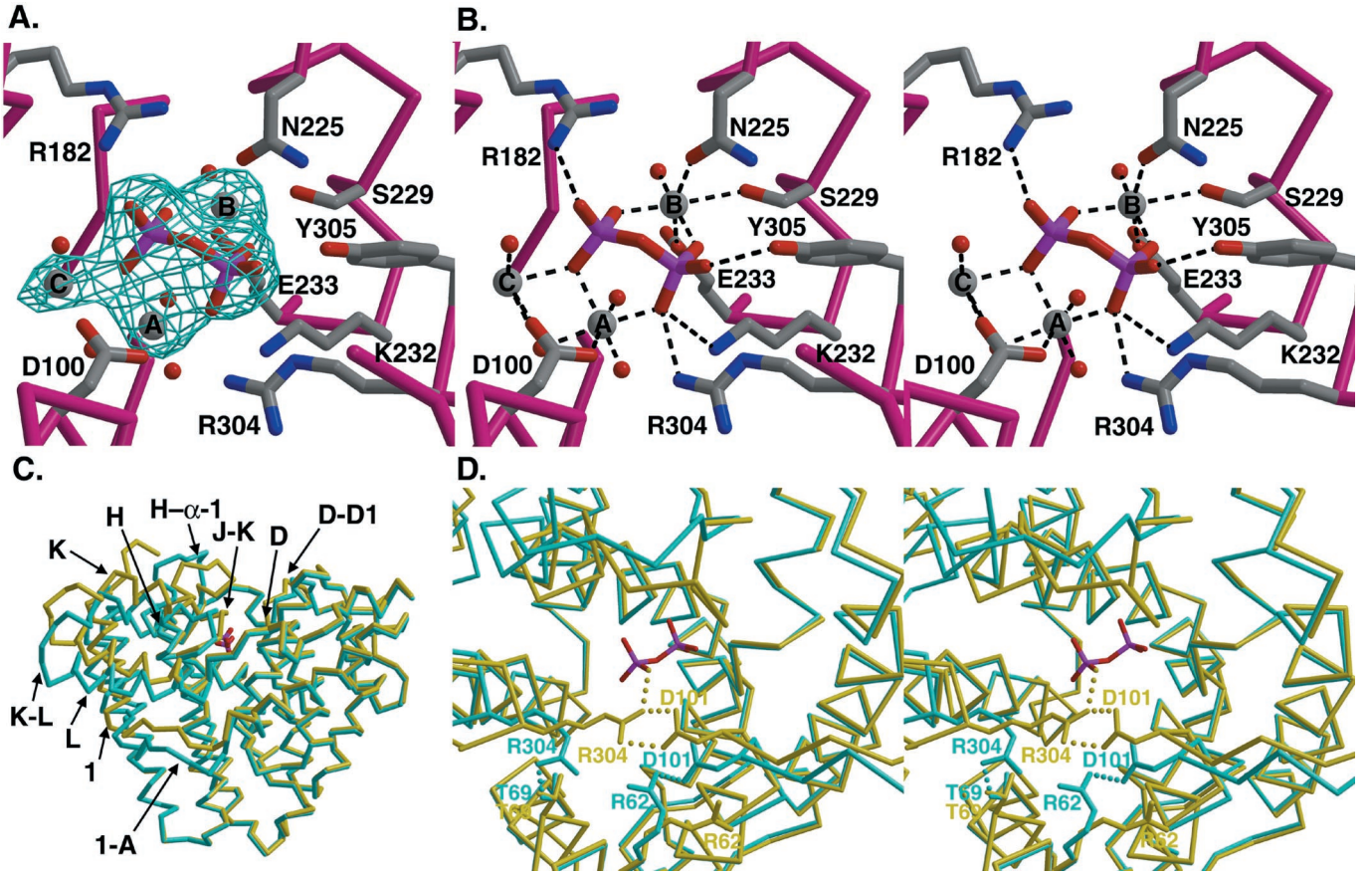

Fig. 4. (*A*) Simulated annealing omit map of the trichodiene synthase-pyrophosphate complex generated with the Fourier coefficients $|F_{obs}| - |F_{calc}|$ and phases calculated from the final model omitting diphosphate and Mg^{2+} ions (contoured at 5σ). Refined atomic coordinates for pyrophosphate, three Mg^{2+} ions (gray spheres), and coordinated water molecules (red spheres) are superimposed. (*B*) Hydrogen bond and metal coordination interactions in the trichodiene synthase-pyrophosphate complex. (*C*) The diphosphate-triggered conformational change is shown by superposition of a C^{α} trace of the unliganded structure (cyan) and the liganded structure (yellow), oriented as shown in Fig. 2*A*. The pyrophosphate molecule (red) is shown for reference. (*D*) View looking directly into the active site reveals that D101 breaks a salt link with R62 to form a new salt link with R304. Because R304 also donates a hydrogen bond to pyrophosphate, this interaction shows how the substrate diphosphate group can trigger a conformational change to cap the active site.

rophosphate also accepts hydrogen bonds from R182 and K232, as well as R304 and Y305 of the basic motif (Fig. 4*B*). The N terminus (M1–P5), helices 1, D, H, J, K, and L, and loops 1-A, D-D1, H–α-1, J-K, and K-L undergo pyrophosphate-triggered conformational changes such that their C^{α} positions move by as much as 6 Å (the rms deviation of 349 C^{α} atoms is 1.4 Å; Fig. 4*C*). These conformational changes are likely triggered by the substrate diphosphate group as well. Intriguingly, after diphosphate binding D101 breaks a poorly oriented salt link with R62 and forms a new salt link with R304 (which breaks a hydrogen bond with T69) that closes the mouth of the active site cleft (Fig. 4*D*); accordingly, mutation of R304 or D101 compromises catalytic activity (20, 21). These conformational changes bring ligand-binding residues closer together, sequester the active site from solvent, and likely trigger diphosphate leaving group departure in catalysis.

Significantly, these ligand-induced conformational changes differ from those observed in other terpene synthases. Conformational changes in 5-*epi*-aristolochene synthase involve the N terminus and loops A-C and J-K (rms deviation of 0.4 Å for 514 C^{α} atoms; ref. 13), and conformational changes in farnesyl diphosphate synthase involve loops F-G, H–α-1, and α-2–α-3 (rms deviation of 0.3–0.9 Å for 367 C^{α} atoms; ref. 32). That these synthases use different protein segments to seal their active sites from solvent during catalysis is intriguing and suggestive of divergent evolution from a common ancestor.

Structure-Based Mechanism. By using the structure of the trichodiene synthase-pyrophosphate complex and the mechanism of trichodiene formation (3, 34–36) as a guide, we have constructed a structure-based model of the trichodiene synthase reaction (Fig. 5). The active site contour is complementary in shape and hydrophobicity to the energy-minimized model of farnesyl diphosphate in its productive conformation (Fig. 5*A* and *B*), and substrate ionization is triggered by diphosphate interactions with R304, K232, R182, Y305, and the Mg^{2+} ions subsequent to active site closure.

Recapture of one of the α-phosphate oxygens by the C3 cation results in the formation of (3*R*)-nerolidyl diphosphate (Fig. 5*C*), conclusively demonstrated to be an intermediate in the reaction (24). Free rotation about the C2–C3 bond from the *transoid* to the *cisoid* conformation orients the empty *p* orbital of C1 in the derived allylic carbocation toward the C6–C7 π orbital to facilitate C1–C6 bond formation subsequent to or concomitant with diphosphate departure. Because the diphosphate moiety plays an important structural role in active site closure, it likely remains bound throughout the cyclization cascade. Bound pyrophosphate also may play an important role in electrostatic stabilization of positively charged carbocationic intermediates during catalysis.

The bisabolyl carbocationic intermediate results with a half-chair cyclohexene conformation (Fig. 5*D*). The C7 carbocation could be stabilized by a cation-π interaction with the side chain

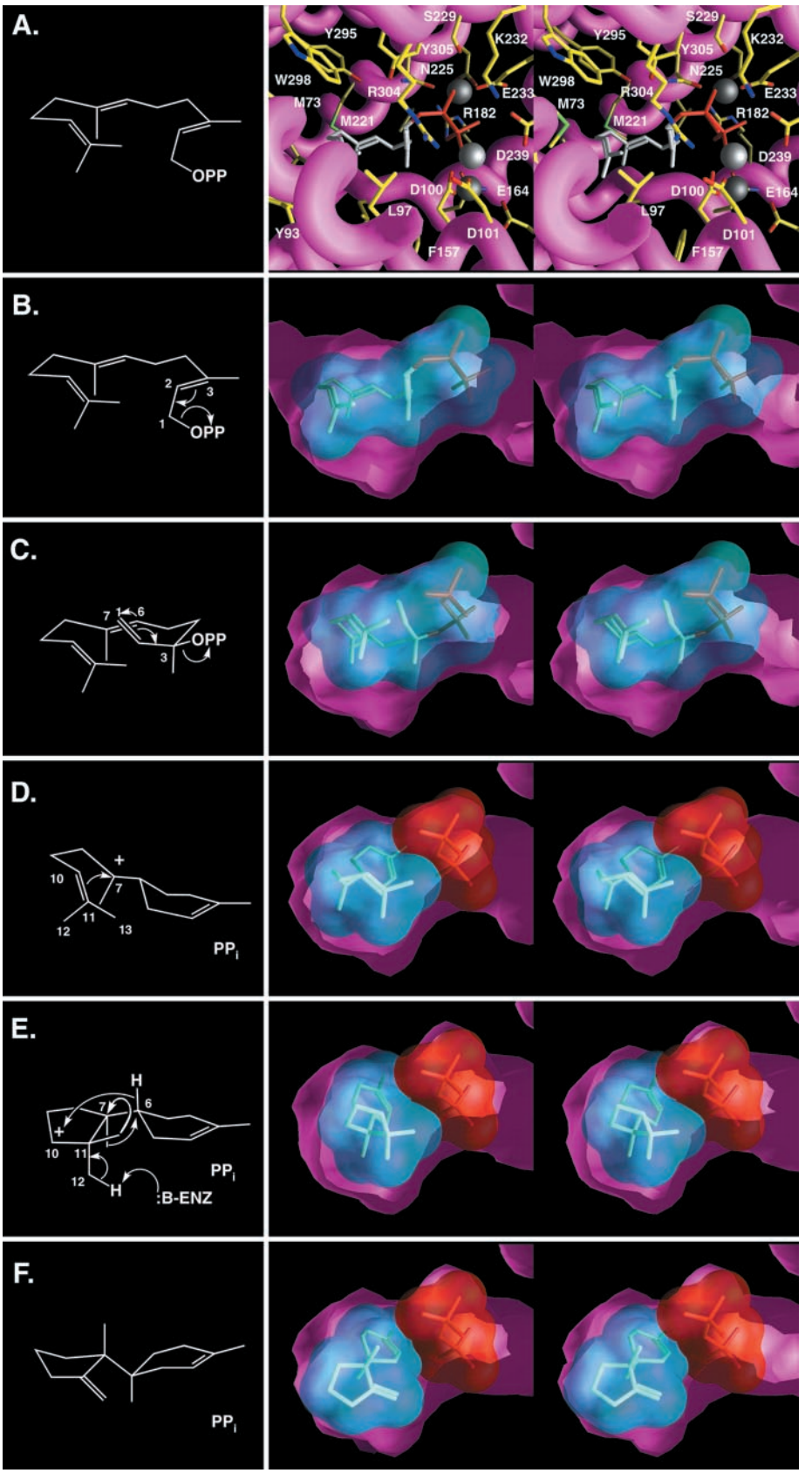

Fig. 5. Model of enzyme-substrate complex showing active site residues (*A*) and van der Waals surfaces (*B*) (protein atoms omitted for clarity). The cyclization cascade proceeds through intermediates nerolidyl diphosphate (*C*), bisabolyl carbocation (*D*), and bicyclic carbocation (*E*) to trichodiene (*F*). OPP, diphosphate; PP_i, pyrophosphate; B-ENZ, catalytic base. The figure was generated with GRASP (40).

of Y93. The cyclohexene ring can rotate such that the empty *p* orbital of C7 is oriented toward the C10–C11 π orbital. After C7–C11 bond formation, the resulting bicyclic secondary carbocation at C10 could be stabilized through long range electrostatic interactions with both D100 and pyrophosphate. Next, three carbocation-driven migrations occur. First, the C6–H migrates to the C10 carbocation through a 1,4-hydride transfer facilitated by the conformation of the intermediate (Fig. 5*E*). The side chain of L97 appears to provide a steric barrier to potentially competing C12 or C13 methyl migration reactions. Two 1,2-methyl migrations subsequently occur: the first from C7 to the carbocation at C6 and the second from C11 to the newly generated carbocation at C7. This second methyl migration is specific for C13, the migration of which may be kinetically favored, because it would provide anchimeric assistance to the departing C7 methyl group; migration of C12 to C7 appears to be sterically hindered by T96. Finally, the C11 carbocation is quenched by proton elimination from C12, possibly mediated either by the carboxylate of D100 or pyrophosphate to yield trichodiene (Fig. 5*F*). Although neither aspartate nor pyrophosphate is strongly basic, either is sufficiently reactive to abstract a proton from the extremely acidic trichodiene carbocation ($pK_a \approx -10$). In turn, protonation of either group could disrupt intermolecular interactions with pyrophosphate, thereby triggering product release.

Variant trichodiene synthases with amino acid substitutions in the diphosphate binding site exhibit altered product specificity (22–24). Changes in the diphosphate position would affect both the proper positioning of the substrate in the active site as well as the substrate-induced conformational change. These structural changes could result in the formation of alternate products because of incorrect folding of the substrate and/or premature quenching of the reaction by solvent.

In conclusion, the x-ray crystal structures of dimeric trichodiene synthase and its complex with pyrophosphate allow us to visualize a putative substrate-induced conformational change involving different secondary structural elements than those implicated in two other sesquiterpene synthases: farnesyl diphosphate synthase (32) and 5-*epi*-aristolochene synthase (13). The trichodiene synthase structures allow us to formulate a structure-based mechanism that rationalizes a wealth of mutagenesis and enzymological data (20–24). Future structural studies of site-specific mutants and enzyme-inhibitor complexes would allow us to test and clarify the mechanism proposed in Fig. 5.

We thank the National Synchrotron Light Source, the Advanced Photon Source, and the Stanford Linear Accelerator Center for beamline access. We thank Drs. Todd Bowser and Hsien-Tai Chiu for helpful scientific discussions. This work was supported by National Institutes of Health Grant GM56838 (to D.W.C.) and Merit Award GM30301 (to D.E.C.).

1. Cane, D. E. (1985) *Acc. Chem. Res.* **18,** 220–226.
2. Croteau, R. & Cane, D. E. (1985) in *Methods in Enzymology: Steroids and Isoprenoids (Part A)*, eds. Law, J. H. & Rilling, H. C. (Academic, New York) Vol. 110, pp. 383–405.
3. Cane, D. E. (1990) *Chem. Rev. (Washington, D.C.)* **90,** 1089–1103.
4. Wendt, K. U. & Schulz, G. E. (1998) *Structure (London)* **6,** 127–133.
5. Lesburg, C. A., Caruthers, J. M., Paschall, C. M. & Christianson, D. W. (1998) *Curr. Opin. Struct. Biol.* **8,** 695–703.
6. Steele, C. L., Crock, J., Bohlmann, J. & Croteau, R. (1998) *J. Biol. Chem.* **273,** 2078–2089.
7. Crock, J., Wildung, M. & Croteau, R. (1997) *Proc. Natl. Acad. Sci. USA* **94,** 12833–12838.
8. Colby, S. M., Crock, J., Dowdle-Rizzo, B., Lemaux, P. G. & Croteau, R. (1998) *Proc. Natl. Acad. Sci. USA* **95,** 2216–2221.
9. Mercke, P., Crock, J., Croteau, R. & Brodelius, P. E. (1999) *Arch. Biochem. Biophys.* **369,** 213–222.
10. Mercke, P., Bengtsson, M., Bouwmeester, H. J., Posthumus, M. A. & Brodelius, P. E. (2000) *Arch. Biochem. Biophys.* **381,** 173–180.
11. Ashby, M. N. & Edwards, P. A. (1990) *J. Biol. Chem.* **265,** 13157–13164.
12. Lesburg, C. A., Zhai, G., Cane, D. E. & Christianson, D. W. (1997) *Science* **277,** 1820–1824.
13. Starks, C. M., Back, K., Chappell, J. & Noel, J. P. (1997) *Science* **277,** 1815–1820.
14. Caruthers, J. M., Kang, I., Rynkiewicz, M. J., Cane, D. E. & Christianson, D. W. (2000) *J. Biol. Chem.* **275,** 25533–25539.
15. Tarshis, L. C., Yan, M., Poulter, C. D. & Sacchettini, J. C. (1994) *Biochemistry* **33,** 10871–10877.
16. Pandit, J., Danley, D. E., Schulte, G. K., Mazzalupo, S., Pauly, T. A., Hayward, C. M., Hamanaka, E. S., Thompson, J. F. & Harwood, H. J. (2000) *J. Biol. Chem.* **275,** 30610–30617.
17. Fujihashi, M., Zhang, Y.-W., Higuchi, Y., Li, X.-Y., Koyama, T. & Miki, K. (2001) *Proc. Natl. Acad. Sci. USA* **98,** 4337–4342. (First Published April 3, 2001; 10.1073/pnas.071514398)
18. Cane, D. E., Swanson, S. & Murthy, P. P. N. (1981) *J. Am. Chem. Soc.* **103,** 2136–2138.
19. Cane, D. E., Wu, Z., Oliver, J. S. & Hohn, T. M. (1993) *Arch. Biochem. Biophys.* **300,** 416–422.
20. Cane, D. E., Shim, J. H., Xue, Q., Fitzsimons, B. C. & Hohn, T. M. (1995) *Biochemistry* **34,** 2480–2488.
21. Cane, D. E., Xue, Q. & Fitzsimons, B. C. (1996) *Biochemistry* **35,** 12369–12376.
22. Cane, D. E., Xue, Q., Van Epp, J. E. & Tsantrizos, Y. S. (1996) *J. Am. Chem. Soc.* **118,** 8499–8500.
23. Cane, D. E. & Xue, Q. (1996) *J. Am. Chem. Soc.* **118,** 1563–1564.
24. Cane, D. E. & Ha, H.-J. (1988) *J. Am. Chem. Soc.* **110,** 6865–6870.
25. Otwinowski, Z. & Minor, W. (1997) in *Methods in Enzymology: Macromolecular Crystallography (Part A)*, eds. Carter, C. W., Jr. & Sweet, R. M. (Academic, New York) Vol. 276, pp. 307–326.
26. Collaborative Computational Project Number 4 (1994) *Acta Crystallogr. D* **50,** 760–763.
27. Cowtan, K. (1994) *Joint CCP4 and ESF-EACBM Newsletter on Protein Crystallography No. 31* (SERC Daresbury Laboratory, Warrington, U.K.), pp. 34–38.
28. Jones, T. A., Zou, J. Y., Cowan, S. W. & Kjeldgaard, M. (1991) *Acta Crystallogr. A* **47,** 110–119.
29. Brünger, A. T., Adams, P. D., Clore, G. M., DeLano, W. L., Gros, P., Grosse-Kunstleve, R. W., Jiang, J.-S., Kuszewski, J., Nilges, M., Pannu, N. S., *et al.* (1998) *Acta Crystallogr. D* **54,** 905–921.
30. Mohamadi, F., Richards, N. G. J., Guida, W. C., Liskamp, R., Lipton, M., Caufield, C., Chang, G., Hendrickson, T. & Still, W. C. (1990) *J. Comput. Chem.* **11,** 440–467.
31. Shindyalov, I. N. & Bourne, P. E. (1998) *Protein Eng.* **11,** 739–747.
32. Tarshis, L. C., Proteau, P. J., Kellogg, B. A., Sacchettini, J. C. & Poulter, C. D. (1996) *Proc. Natl. Acad. Sci. USA* **93,** 15018–15023.
33. Cane, D. E. & Kang, I. (2000) *Arch. Biochem. Biophys.* **376,** 354–364.
34. Cane, D. E. & Yang, G. (1994) *J. Org. Chem.* **59,** 5794–5798.
35. Cane, D. E., Yang, G., Xue, Q. & Shim, J. H. (1995) *Biochemistry* **34,** 2471–2479.
36. Cane, D. E., Chiu, H.-T., Liang, P.-H. & Anderson, K. S. (1997) *Biochemistry* **36,** 8332–8339.
37. Kraulis, P. J. (1991) *J. Appl. Crystallogr.* **24,** 946–950.
38. Bacon, D. & Anderson, W. F. (1988) *J. Mol. Graphics* **6,** 219–220.
39. Merritt, E. A. & Murphy, M. E. P. (1994) *Acta Crystallogr. D* **50,** 869–873.
40. Nicholls, A., Sharp, K. A. & Honig, B. (1991) *Proteins* **11,** 281–296.